Band-filling-controlled magnetism from transition metal intercalation in $N_{1/3}NbS_2$ revealed with first-principles calculations

Z. Hawkhead,[1] T. J. Hicken,[1,2,3] N. P. Bentley,[1] B. M. Huddart,[1,4] S. J. Clark,[1] and T. Lancaster[1]
[1]*Department of Physics, Centre for Materials Physics, Durham University, Durham DH1 3LE, United Kingdom*
[2]*Department of Physics, Royal Holloway, University of London, Egham TW20 0EX, United Kingdom*
[3]*Laboratory for Muon Spin Spectroscopy, PSI, 5232 Villigen, Switzerland*
[4]*Department of Physics, Clarendon Laboratory, University of Oxford, Parks Road, Oxford OX1 3PU, United Kingdom*

(Received 15 May 2023; accepted 10 October 2023; published 6 November 2023)

We present a first-principles study of the effect of 3*d* transition metal intercalation on the magnetic properties of the 2*H*-NbS_2 system, using spin-resolved density functional theory calculations to investigate the electronic structure of $N_{1/3}NbS_2$ (N = Ti, V, Cr, Mn, Fe, Co, Ni). We are able to accurately determine the magnetic moments and crystal-field splitting, and find that the magnetic properties of the materials are determined by a mechanism based on filling rigid bands with electrons from the intercalant. We predict the dominant magnetic interaction of these materials by considering Fermi-surface topology, finding agreement with experiment where data are available.

DOI: 10.1103/PhysRevMaterials.7.114002

I. INTRODUCTION

The transition metal dichalcogenides (TMDCs) (MX_2, where M is a transition metal and X is a chalcogen) [1–4] have earned attention over the decades for their interesting physical properties such as charge-density waves [5–8], superconductivity [9–11], thickness-dependent transport properties [12,13], and tunable band gaps [14]. Recently, they have garnered interest for potential applications in novel low-dimensional devices such as atomically thin transistors [3]. To further modify the properties, the layered van der Waals structure allows for the intercalation of other species between the TMDC layers. In this paper, we present spin-resolved density functional theory (spin-DFT) calculations that elucidate the effects of intercalating the TMDCs with first-period 3*d* transition metal atoms in the form $N_{1/3}MS_2$, where N is the intercalant. Broadly in line with a rigid-band picture [15,16], we find that the spin-resolved electronic bands remain quite static across the series, and that the ordered spin-magnetic moment is determined by filling these crystal-field-split bands with electrons from the intercalant. The resulting Fermi-surface topology provides an explanation for the difference in dominant magnetic interactions seen in the series. Finally, a density of states (DOS) analysis shows that the pseudogapped structure giving rise to the low-temperature properties of the N = Cr material [17,18] should not be expected to occur near the Fermi level in other members of the series, implying that their low-temperature dynamics will be significantly different. Where experimental comparisons are available, we find our results agree favorably in all cases.

The structure of $N_{1/3}MS_2$ is shown in Fig. 1. Intercalating first-period transition metals into NbS_2 gives ten possible materials. Some of these have been synthesized and widely studied; others were subjected to relatively little attention, in part due to the difficult synthesis. The determination of the magnetic structure has been at the forefront of the effort to measure their properties, with structures so far determined for N = V [19–21], Cr [22], Mn [23,24], Fe [25–27], Co, [28,29] and Ni [15]. The systems can be grouped into those hosting a ferromagnetic (N = V, Mn, and Cr) or antiferromagnetic (N = Co, Ni, Fe) exchange interaction. Notably, among intercalants in the first half of the period, a ferromagnetic interaction is preferred, whereas in the second half of the period, it is more commonly antiferromagnetic. Of the intercalated TMDCs, the most well studied is $Cr_{1/3}NbS_2$, which hosts a long-wavelength chiral helimagnetic ground state [22,30,31] with a near-ferromagnetic alignment of spins, and exotic magnetic textures in the applied magnetic field. Moreover, the discovery of a topologically nontrivial chiral soliton lattice (regions of helimagnetism separated by ferromagnetism) on application of a magnetic field, first in $Cr_{1/3}NbS_2$ [17,23,24,27,31,32] and later in $Cr_{1/3}TaS_2$ [33], has renewed interest in this material class.

Density functional theory (DFT) techniques have become increasingly useful for the study of long-range chiral magnetism over recent years [34,35]. It was originally suggested that the photoemission and optical properties of the TMDC materials could be described using a rigid-band approximation of the electronic structure, in which intercalation leads to a transfer of charge between the intercalant species and the *d* conduction band of the host lattice, while the shape and ordering of the valence bands remains approximately the same [15,16]. More recent first-principles calculations using

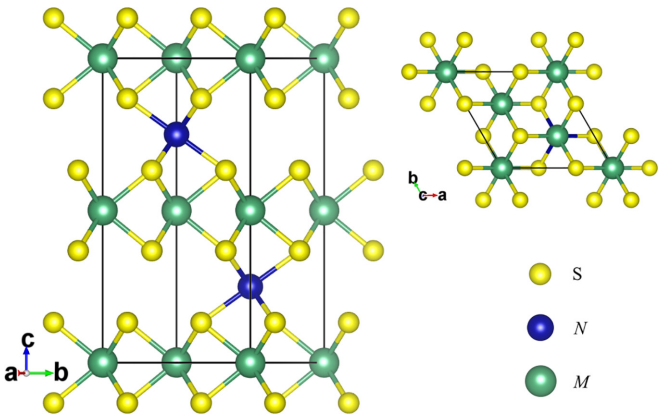

FIG. 1. Crystal structure of the intercalated TMDCs. The chemical form is $N_{1/3}MS_2$, where N are the intercalated atoms.

spin-DFT concentrating on the N = Cr material [17,18] highlight a drop in the density of states (DOS) at the Fermi level that contributes to the transport and magnetic properties at low temperatures.

II. COMPUTATIONAL METHODS

We performed spin-DFT calculations of the electronic structure of $N_{1/3}NbS_2$, where N is a transition metal in the first period, using the plane-wave pseudopotential code CASTEP [36,37]. To more directly compare the electronic structure across the series, each calculation was initialized in a ferromagnetic state with a moment on the N ions. Despite experimental evidence that some of these materials exhibit some degree of antiferromagnetic interactions in their ground state, we are only able to stabilize ferromagnetically ordered states, suggesting that this may be a stable higher-energy configuration for some of the systems. To capture some of the correlation effects that often contribute to long-range magnetic order, we included a small Hubbard U of 2.0–2.5 eV (3.5 eV for N = Ni) on the N d orbitals for most materials. These values were chosen as the smallest value required to form a ferromagnetic state in each material (below this U the calculations typically result in a nonmagnetic state). It was not possible to stabilize an ordered moment at any physically plausible value of U for N = Sc, Cu, and Zn.

III. ELECTRONIC STRUCTURE AND BAND FILLING

Our results imply that the magnetic properties of the intercalated TMDCs follow a simple band-filling mechanism similar to the rigid-band approximation [16]. The band structures of $N_{1/3}NbS_2$ are shown in Figs. 2(a)–2(g). We note that as we progress from $Ti_{1/3}NbS_2$ through to $Mn_{1/3}NbS_2$, (top of Fig. 2) the band structure of the spin-down electrons (blue) remains essentially static while the position of some spin-up electron bands shift with respect to the Fermi energy (E_F). Conversely, the effect is seen with the spin species reversed for $Fe_{1/3}NbS_2$ through to $Ni_{1/3}NbS_2$, although this is less prominent for the latter materials. The changes to the bands contributing to the magnetic moment are characterized in Fig. 2(h). We show how a characteristic energy of the N 3d bands (calculated as a weighted average of the energy of the d bands at the Γ point) changes as the number of outer electrons is increased, demonstrating the band shifting discussed above. In the first half of the period, the energy of the N 3d spin-down

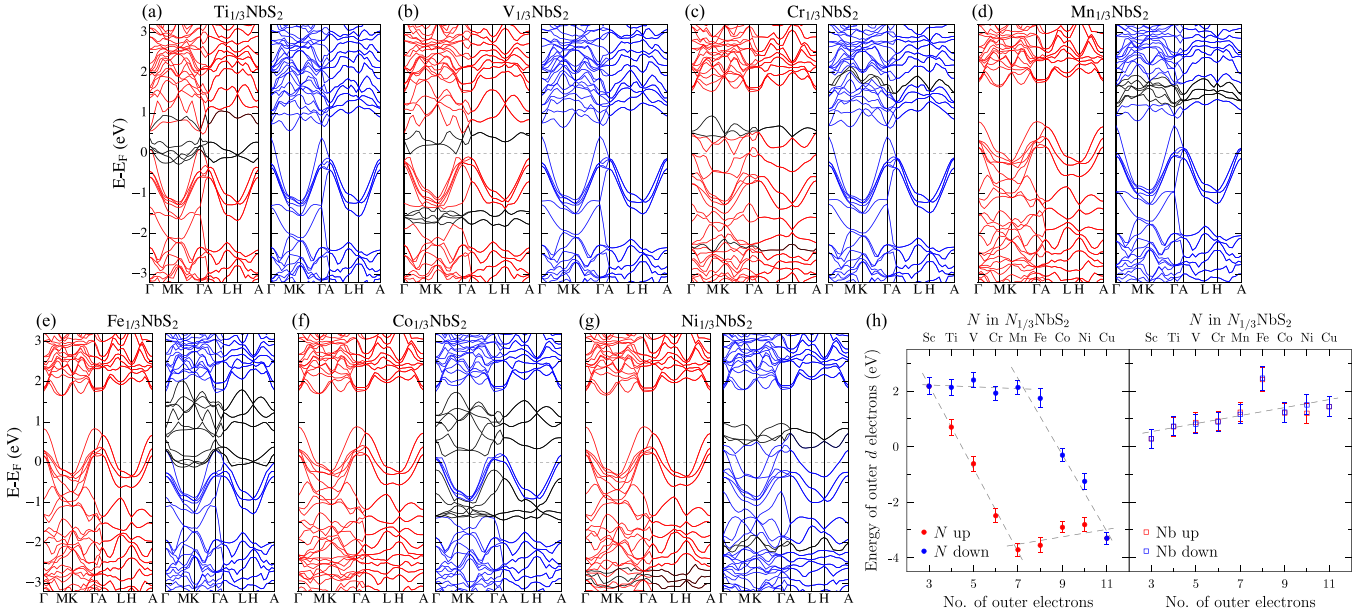

FIG. 2. (a)–(g) Band structures of the TMDCs as a function of intercalated transition metal calculated along a labeled high-symmetry path. The band structures arranged in order of increasing unpaired electrons in the transition metal outer shell. Spin-up channels are shown in red and spin-down channels are shown in blue. The highlighted bands (black) correspond to orbitals with majority d character associated with the intercalant. The energy dependence of the d orbitals can also be seen in the Supplemental Material (SM) [38] (see also Refs. [17,19,21,22,24,25,39–47] within). (h) The average band energy at the Γ point weighted by the proportion of N d-orbital character as a function of the number of electrons in the outer shell of the intercalant. Gray dashed lines are a guide to the eye.

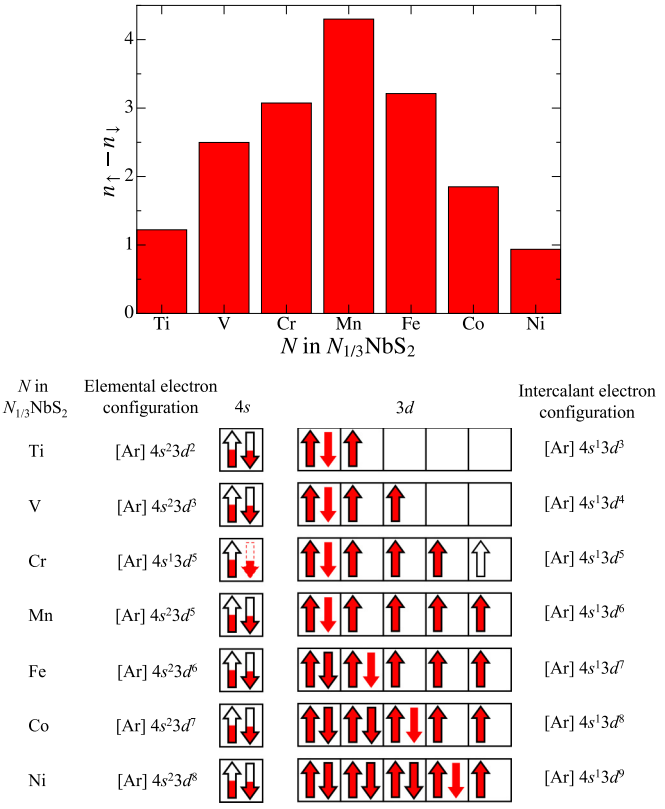

FIG. 3. Top: Spin-up ($n_\uparrow$) minus spin-down ($n_\downarrow$) electrons in $3d$ orbitals of N in $N_{1/3}NbS_2$. Bottom: Schematic of the band-filling mechanism in the $4s$ and $3d$ orbitals of the intercalated transition metal compared to the elemental electronic configurations. Red arrows indicate the calculated electron occupation while black outlines show the elemental occupation. There is some hybridization of the $4s$ and $4p$ orbitals in each material, with ≈1 electron shared across both spin-up and spin-down orbitals. The $4p$ orbitals are omitted for clarity.

bands remains essentially static while the N $3d$ spin-up bands decrease in energy. In the second half of the period, the N $3d$ spin-down band energies decrease while the spin-up band energies increase slightly. In contrast, we see that the characteristic energy of the Nb bands [Fig. 2(h) (right)] is essentially static as we increase the number of electrons, with little energy difference between the spin-up and spin-down band energies. This highlights that the magnetic behaviors in these materials are dominated by the intercalant. We can see in Fig. 2(h) that the two distinct regions in the spin-up and spin-down energies intersect for $Sc_{1/3}NbS_2$ and $Cu_{1/3}NbS_2$ such that the spin-up and spin-down energy levels are equal, consistent with the lack of an overall moment found in these materials.

The static nature of a subset of the bands in the band structure has consequences for the spin found on the magnetic ions [Fig. 3 (top)]. By projecting the electron density onto the atomic orbitals by Mulliken analysis [48], we see that for the materials where the intercalant has a less-than-half-filled $3d$ shell, the spin increases across the series, and then begins to drop again as we move to the materials with a more than half-filled shell. In the first half of the period, we add approximately one electron to the spin-up subshells.

TABLE I. The magnetic moment of $N_{1/3}NbS_2$. Calculations are from the idealized model shown in Fig. 3. n is the number of unpaired electrons in the $3d$ orbitals, such that the spin-only moment $\mu_s = \sqrt{n(n+2)}$. Experimental moments are an average (with a standard error when more than one value is available) of data from Refs. [19,21,22,24,25,40–46].

	Model		Experiment		Model		Experiment
M	n	μ_s (μ_B)	$\mu_{expt.}$ (μ_B)	M	n	μ_s (μ_B)	$\mu_{expt.}$ (μ_B)
Sc	0	0	–	Fe	3	3.87	4.8(2)
Ti	1	1.73	1.76	Co	2	2.83	3.0(5)
V	2	2.83	2.93(3)	Ni	1	1.73	2.4(3)
Cr	3	3.87	3.6(2)	Cu	0	0	–
Mn	4	4.90	5.1(2)	Zn	0	0	–

Once the spin-up shells are filled (at N = Mn) we start filling the spin-down shells, explaining the decrease in spin as we approach the end of the series. We also see that there is just less than one electron populating the spin-down shells of the magnetic ions in the first half of the period (0.81, 0.70, 0.97, and 0.67 for N = Ti, V, Cr, and Mn respectively). This is not what one would expect from a simple Hund's rules analysis and points to crystal-field effects (see below). The resulting picture, illustrated in Fig. 3 (bottom), can be extrapolated to demonstrate that the N = Sc, Cu, and Zn systems will not have any unpaired spins in the $3d$ orbitals, explaining why they are found not to host an ordered moment (see Table I). Notably, we also find that the electron filling in N = Cr differs from that found in elemental Cr. The elemental transition metals in the first period have a similar electronic structure, with the $4s$ shell filled and each having an extra $3d$ electron than the previous element. However, this is not the case for elemental Cr, where it is energetically favorable to instead half-fill the $3d$ band, resulting in a composition of $[Ar]4s^1 3d^5$. Instead, $Cr_{1/3}NbS_2$ follows the pattern of the other materials in the series, consistent with a significant crystal field splitting.

The space group for the intercalated TMDCs is $P6_322$ and the intercalants occupy the $2c$ Wyckoff site, which has local site symmetry of 3.2 (corresponding to the D_3 point group). This environment splits the intercalant levels into $a_1 + 2e$, where the irreducible representation a_1 corresponds to the d_{z^2} orbital, and $2e$ corresponds to the d_{xz}, d_{yz}, d_{xy}, and $d_{x^2-y^2}$ orbitals. The overlap of the intercalant $3d$ orbitals and the sulfur p orbitals results in the d_{z^2} orbital being lower in energy than the other orbitals. By calculating the partial DOS (PDOS) for this series, we find that the d_{z^2} orbitals of the intercalant are indeed lower in energy than the other d orbitals, with the majority of the DOS associated with this orbital sitting approximately 1.5 eV below the Fermi energy in these materials (see SM [38]). Capturing and quantifying these important crystal-field effects increases confidence that our calculations are a faithful reflection of the underlying electronic structure.

We compare our calculations to experimentally measured magnetic moments by computing the spin-only magnetic moment. Beal [44] suggested that these materials are orbitally quenched, hence the spin-only moment is a good description of the realized magnetic moment. In Tab. I we show the spin-only moment calculated using the model filling pattern shown

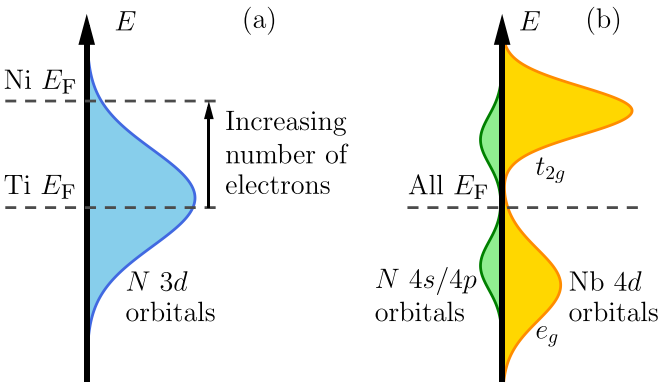

FIG. 4. Schematic diagram demonstrating how the Fermi energy (E_F) changes with respect to the non-spin-resolved DOS in $N_{1/3}NbS_2$ (N = Ti, V, Mn, Fe, Co, Ni). (a) DOS of N 3d electrons: The DOS stays roughly static while E_F increases with added electrons. (b) DOS of N 4s/p and Nb 4d electrons: The DOS stay constant with respect to E_F.

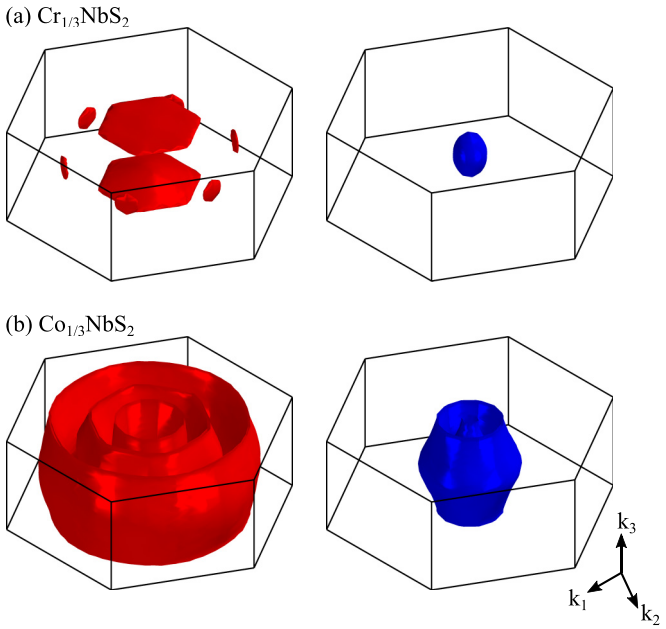

FIG. 5. Fermi surfaces of (a) $Cr_{1/3}NbS_2$ and (b) $Co_{1/3}NbS_2$ showing contributions from the spin-up (red) and spin-down (blue) electrons.

in Fig. 3 (bottom). (A similar comparison from the Mulliken spin can be found in SM [38].) While there is a slightly greater deviation between the calculated spin-only moments and the experimental values where there is a wider range of moments reported experimentally, especially in the materials with a reported antiferromagnetic exchange, we find good agreement with our calculations.

The calculated DOS of $N_{1/3}NbS_2$ (N = Ti, V, Cr, Mn, Fe, Co, Ni) show marked similarities in either the spin-down (N = Ti, V, Cr, and Mn) or spin-up channels (N = Fe, Co, and Ni) [38]. We illustrate the effects in Fig. 4. The changes to the DOS are dominated by the N 3d bands. As we increase the number of electrons by including heavier intercalants, we see that E_F increases relative to the N 3d partial DOS. However, the nonmagnetic bands comprising the N 4s/p electrons stay fixed with respect to the changing E_F. The Nb 4d orbitals also undergo splitting due to the presence of crystal fields, with the e_g states below E_F and the t_{2g} states above. There are approximately four filled 4d states while six states remain unfilled. We find that there is little DOS at E_F due to the Nb 4d states. Xie *et al.* [27] argue from symmetry considerations that there should be a partially filled Nb 4d_{z^2} orbital, however, this is inconsistent with our first-principles calculations.

Our previous study of $Cr_{1/3}NbS_2$ found a depression in the DOS at E_F in one spin channel [17]. This pseudogap is responsible for unusual low-temperature dynamics. However, our present results show that as a result of the band-filling mechanism, this pseudogap is not found at E_F for any of the other materials considered. We conclude that, rather than being a feature of the class of materials, intercalation with Cr is required for pseudogap-driven physics. This seems to be borne out by recent experiments on the N = V and Mn systems [21,24,47].

It is notable that the systems with more than half-full 3d shells (N = Fe, Co, and Ni) have been reported to have ground states with some antiferromagneticlike character, rather than the ferromagnetic one in our calculations. Insight into this is provided by the topology of the Fermi surfaces across the series, examples of which are shown in Fig. 5. (Further such Fermi surfaces can be seen in SM [38].) For N = Fe, Co, and Ni, the Fermi surface has a quasi-two-dimensional character. This reduced dimensionality leads to an increased influence of electronic instabilities, caused for example by Fermi-surface nesting or strong Coulomb interactions of the 4d band of the Nb atom [49]. This could cause (antiferromagnetic) spin-density-wave formation and a consequent reconstruction of the Fermi surface. In contrast, the materials with N = Ti, V, and Cr appear far more three dimensional, and have a ferromagnetic exchange interaction, with the N = Mn system lying somewhere in between.

IV. CONCLUSIONS

Our first-principles study into the magnetic properties of the intercalated TMDCs demonstrates that a rigid-band picture of the electronic structure largely explains the magnetism of the system. Using a simple ferromagnetic model for all the materials in this series, we are able to accurately reproduce experimental observations and describe the underlying electronic structure. We find that the degeneracy of the 3d orbitals is broken such that the electron filling pattern, distinct from that of the isolated intercalant, is consistent with the local symmetry of the crystal and correctly predicts the magnetic moment. The calculated Fermi surfaces provide insight into the exchange interaction that manifests in the systems. Our work demonstrates that, in this class of materials, not only do first-principles calculations lead to unique insights, but they are sufficiently successful at predicting experimental results that they could be used as a cost-effective technique for screening materials for desired properties before crystal synthesis is required.

ACKNOWLEDGMENTS

We thank A. Hall, C. Wang, and L. Yu for useful discussion. We acknowledge the support of EPSRC (UK) (EP/N032128/1) and Durham Hamilton HPC. Research data will be made available via Durham Collections [50].

[1] S. Manzeli, D. Ovchinnikov, D. Pasquier, O. V. Yazyev, and A. Kis, 2D transition metal dichalcogenides, Nat. Rev. Mater. **2**, 17033 (2017).

[2] Z. Wei, B. Li, C. Xia, Y. Cui, J. He, J.-B. Xia, and J. Li, Various structures of 2D transition-metal dichalcogenides and their applications, Small Methods **2**, 1800094 (2018).

[3] Q. H. Wang, K. Kalantar-Zadeh, A. Kis, J. N. Coleman, and M. S. Strano, Electronics and optoelectronics of two-dimensional transition metal dichalcogenides, Nat. Nanotechnol. **7**, 699 (2012).

[4] K. F. Mak, C. Lee, J. Hone, J. Shan, and T. F. Heinz, Atomically thin MoS_2: A new direct-gap semiconductor, Phys. Rev. Lett. **105**, 136805 (2010).

[5] J. A. Wilson and A. Yoffe, The transition metal dichalcogenides discussion and interpretation of the observed optical, electrical and structural properties, Adv. Phys. **18**, 193 (1969).

[6] D. Moncton, J. Axe, and F. DiSalvo, Study of superlattice formation in $2H$-$NbSe_2$ and $2H$-$TaSe_2$ by neutron scattering, Phys. Rev. Lett. **34**, 734 (1975).

[7] O. Rajora and A. Curzon, The preparation and x-ray diffraction study of the layer materials NbS_xSe_{2-x} for $0 \leqslant x \leqslant 2$, Phys. Status Solidi A **99**, 65 (1987).

[8] M. Naito and S. Tanaka, Electrical transport properties in $2H$-NbS_2, -$NbSe_2$, -TaS_2 and -$TaSe_2$, J. Phys. Soc. Jpn. **51**, 219 (1982).

[9] V. G. Tissen, M. R. Osorio, J.-P. Brison, N. M. Nemes, M. García-Hernández, L. Cario, P. Rodiere, S. Vieira, and H. Suderow, Pressure dependence of superconducting critical temperature and upper critical field of $2H$-NbS_2, Phys. Rev. B **87**, 134502 (2013).

[10] C. Heil, S. Poncé, H. Lambert, M. Schlipf, E. R. Margine, and F. Giustino, Origin of superconductivity and latent charge density wave in NbS_2, Phys. Rev. Lett. **119**, 087003 (2017).

[11] C. Witteveen, K. Górnicka, J. Chang, M. Månsson, T. Klimczuk, and F. O. von Rohr, Polytypism and superconductivity in the NbS_2 system, Dalton Trans. **50**, 3216 (2021).

[12] A. Castellanos-Gomez, M. Barkelid, A. Goossens, V. E. Calado, H. S. van der Zant, and G. A. Steele, Laser-thinning of MoS_2: On demand generation of a single-layer semiconductor, Nano Lett. **12**, 3187 (2012).

[13] R. Ganatra and Q. Zhang, Few-layer MoS_2: A promising layered semiconductor, ACS Nano **8**, 4074 (2014).

[14] A. Ramasubramaniam, D. Naveh, and E. Towe, Tunable band gaps in bilayer transition-metal dichalcogenides, Phys. Rev. B **84**, 205325 (2011).

[15] C. Battaglia, H. Cercellier, L. Despont, C. Monney, M. Prester, H. Berger, L. Forró, M. Garnier, and P. Aebi, Non-uniform doping across the Fermi surface of NbS_2 intercalates, Eur. Phys. J. B **57**, 385 (2007).

[16] W. Clark, Structural and photoemission studies of some transition metal intercalates of NbS_2, J. Phys. C: Solid State Phys. **9**, L693 (1976).

[17] T. J. Hicken, Z. Hawkhead, M. N. Wilson, B. M. Huddart, A. E. Hall, G. Balakrishnan, C. Wang, F. L. Pratt, S. J. Clark, and T. Lancaster, Energy-gap driven low-temperature magnetic and transport properties in $Cr_{1/3}MS_2$ (M = Nb, Ta), Phys. Rev. B **105**, L060407 (2022).

[18] N. J. Ghimire, M. A. McGuire, D. S. Parker, B. Sipos, S. Tang, J.-Q. Yan, B. C. Sales, and D. Mandrus, Magnetic phase transition in single crystals of the chiral helimagnet $Cr_{1/3}NbS_2$, Phys. Rev. B **87**, 104403 (2013).

[19] S. S. P. Parkin and R. H. Friend, $3d$ transition-metal intercalates of the niobium and tantalum dichalcogenides. I. Magnetic properties, Philos. Mag. B **41**, 65 (1980).

[20] S. S. P. Parkin and R. H. Friend, $3d$ transition-metal intercalates of the niobium and tantalum dichalcogenides. II. Transport properties, Philos. Mag. B **41**, 95 (1980).

[21] A. E. Hall, D. D. Khalyavin, P. Manuel, D. A. Mayoh, F. Orlandi, O. A. Petrenko, M. R. Lees, and G. Balakrishnan, Magnetic structure investigation of the intercalated transition metal dichalcogenide $V_{1/3}NbS_2$, Phys. Rev. B **103**, 174431 (2021).

[22] T. Moriya and T. Miyadai, Evidence for the helical spin structure due to antisymmetric exchange interaction in $Cr_{1/3}NbS_2$, Solid State Commun. **42**, 209 (1982).

[23] Y. Kousaka, Y. Nakao, J. Kishine, M. Akita, K. Inoue, and J. Akimitsu, Chiral helimagnetic order in $T_{1/3}NbS_2$ (T = Cr, Mn), Nucl. Instrum. Methods Phys. Res. Sect. A **600**, 250 (2009).

[24] A. E. Hall, J. C. Loudon, P. A. Midgley, A. C. Twitchett-Harrison, S. J. R. Holt, D. A. Mayoh, J. P. Tidey, Y. Han, M. R. Lees, and G. Balakrishnan, Comparative study of the structural and magnetic properties of $Mn_{1/3}NbS_2$ and $Cr_{1/3}NbS_2$, Phys. Rev. Mater. **6**, 024407 (2022).

[25] B. Van Laar, H. Rietveld, and D. Ijdo, Magnetic and crystallographic structures of Me_xNbS_2 and Me_xTaS_2, J. Solid State Chem. **3**, 154 (1971).

[26] A. Little, C. Lee, C. John, S. Doyle, E. Maniv, N. L. Nair, W. Chen, D. Rees, J. W. Venderbos, R. M. Fernandes *et al.*, Three-state nematicity in the triangular lattice antiferromagnet $Fe_{1/3}NbS_2$, Nat. Mater. **19**, 1062 (2020).

[27] L. S. Xie, S. Husremović, O. Gonzalez, I. M. Craig, and D. K. Bediako, Structure and magnetism of iron- and chromium-intercalated niobium and tantalum disulfides, J. Am. Chem. Soc. **144**, 9525 (2022).

[28] S. Parkin, E. Marseglia, and P. Brown, Magnetic structure of $Co_{1/3}NbS_2$ and $Co_{1/3}TaS_2$, J. Phys. C: Solid State Phys. **16**, 2765 (1983).

[29] G. Tenasini, E. Martino, N. Ubrig, N. J. Ghimire, H. Berger, O. Zaharko, F. Wu, J. F. Mitchell, I. Martin, L. Forró, and A. F. Morpurgo, Giant anomalous Hall effect in quasi-two-dimensional layered antiferromagnet $Co_{1/3}NbS_2$, Phys. Rev. Res. **2**, 023051 (2020).

[30] T. Miyadai, K. Kikuchi, H. Kondo, S. Sakka, M. Arai, and Y. Ishikawa, Magnetic properties of $Cr_{1/3}NbS_2$, J. Phys. Soc. Jpn. **52**, 1394 (1983).

[31] Y. Kousaka, T. Ogura, J. Zhang, P. Miao, S. Lee, S. Torii, T. Kamiyama, J. Campo, K. Inoue, and J. Akimitsu, Long periodic helimagnetic ordering in CrM_3S_6 (M = Nb and Ta), J. Phys.: Conf. Ser. **746**, 012061 (2016).

[32] Y. Togawa, T. Koyama, K. Takayanagi, S. Mori, Y. Kousaka, J. Akimitsu, S. Nishihara, K. Inoue, A. S. Ovchinnikov, and J. Kishine, Chiral magnetic soliton lattice on a chiral helimagnet, Phys. Rev. Lett. **108**, 107202 (2012).

[33] C. Zhang, J. Zhang, C. Liu, S. Zhang, Y. Yuan, P. Li, Y. Wen, Z. Jiang, B. Zhou, Y. Lei *et al.*, Chiral helimagnetism and one-dimensional magnetic solitons in a Cr-intercalated transition metal dichalcogenide, Adv. Mater. **33**, 2101131 (2021).

[34] T. J. Hicken, M. N. Wilson, K. J. A. Franke, B. M. Huddart, Z. Hawkhead, M. Gomilšek, S. J. Clark, F. L. Pratt, A. Štefančič, A. E. Hall, M. Ciomaga Hatnean, G. Balakrishnan, and T. Lancaster, Megahertz dynamics in skyrmion systems probed with muon-spin relaxation, Phys. Rev. B **103**, 024428 (2021).

[35] T. J. Hicken, M. N. Wilson, S. J. R. Holt, R. Khassanov, M. R. Lees, R. Gupta, D. Das, G. Balakrishnan, and T. Lancaster, Magnetism in the Néel-skyrmion host GaV_4S_8 under pressure, Phys. Rev. B **105**, 134414 (2022).

[36] S. J. Clark, M. D. Segall, C. J. Pickard, P. J. Hasnip, M. J. Probert, K. Refson, and M. Payne, First principles methods using CASTEP, Z. Kristallogr. **220**, 567 (2005).

[37] J. R. Yates, X. Wang, D. Vanderbilt, and I. Souza, Spectral and Fermi surface properties from Wannier interpolation, Phys. Rev. B **75**, 195121 (2007).

[38] See Supplemental Material at http://link.aps.org/supplemental/10.1103/PhysRevMaterials.7.114002 for further details that would allow one to reproduce our work, additional comparison to experimental measurements, DOS calculations for the materials in the series, and a complete set of Fermi surfaces.

[39] J. P. Perdew, K. Burke, and M. Ernzerhof, Generalized gradient approximation made simple, Phys. Rev. Lett. **77**, 3865 (1996).

[40] J. Van den Berg and P. Cossee, Structural aspects and magnetic behaviour of NbS_2 and TaS_2 containing extra metal atoms of the first transition series, Inorg. Chim. Acta **2**, 143 (1968).

[41] K. Anzenhofer, J. Van Den Berg, P. Cossee, and J. Helle, The crystal structure and magnetic susceptibilities of $MnNb_3S_6$, $FeNb_3S_6$, $CoNb_3S_6$ and $NiNb_3S_6$, J. Phys. Chem. Solids **31**, 1057 (1970).

[42] F. Hulliger and E. Pobitschka, On the magnetic behavior of new $2H$-NbS_2-type derivatives, J. Solid State Chem. **1**, 117 (1970).

[43] R. Friend, A. Beal, and A. Yoffe, Electrical and magnetic properties of some first row transition metal intercalates of niobium disulphide, Philos. Mag. **35**, 1269 (1977).

[44] A. R. Beal, The first row transition metal intercalation complexes of some metallic group VA transition metal dichalcogenides, in *Intercalated Layered Materials*, edited by F. Lévy (Springer, Berlin, 1979), pp. 251–305.

[45] O. Gorochov, A. L. Blanc-soreau, J. Rouxel, P. Imbert, and G. Jehanno, Transport properties, magnetic susceptibility and Mössbauer spectroscopy of $Fe_{0.25}NbS_2$ and $Fe_{0.33}NbS_2$, Philos. Mag. B **43**, 621 (1981).

[46] S. C. Haley, S. F. Weber, T. Cookmeyer, D. E. Parker, E. Maniv, N. Maksimovic, C. John, S. Doyle, A. Maniv, S. K. Ramakrishna *et al.*, Half-magnetization plateau and the origin of threefold symmetry breaking in an electrically switchable triangular antiferromagnet, Phys. Rev. Res. **2**, 043020 (2020).

[47] S. K. Karna, F. N. Womack, R. Chapai, D. P. Young, M. Marshall, W. Xie, D. Graf, Y. Wu, H. Cao, L. DeBeer-Schmitt, P. W. Adams, R. Jin, and J. F. DiTusa, Consequences of magnetic ordering in chiral $Mn_{1/3}NbS_2$, Phys. Rev. B **100**, 184413 (2019).

[48] R. S. Mulliken, Electronic population analysis on LCAO–MO molecular wave functions. I, J. Chem. Phys. **23**, 1833 (1955).

[49] F. Güller, V. L. Vildosola, and A. M. Llois, Spin density wave instabilities in the NbS_2 monolayer, Phys. Rev. B **93**, 094434 (2016).

[50] 10.15128/r19s1616247.